JACS
JOURNAL OF THE AMERICAN CHEMICAL SOCIETY
Article
pubs.acs.org/JACS

# Unification of Catalytic Water Oxidation and Oxygen Reduction Reactions: Amorphous Beat Crystalline Cobalt Iron Oxides

Arindam Indra,[†] Prashanth W. Menezes,[†] Nastaran Ranjbar Sahraie,[‡] Arno Bergmann,[‡] Chittaranjan Das,[§] Massimo Tallarida,[§] Dieter Schmeißer,[§] Peter Strasser,*[,‡,⊥] and Matthias Driess*[,†]

[†]Metalorganics and Inorganic Materials, Department of Chemistry, Technische Universität Berlin, Straße des 17 Juni 135, Sekr. C2, 10623 Berlin, Germany

[‡]The Electrochemical Energy, Catalysis, and Materials Science Group, Department of Chemistry, Technische Universität Berlin, Straße des 17 Juni 124, Sekr. TC3, 10623 Berlin, Germany

[§]Applied Physics and Sensors, Brandenburg University of Technology Cottbus, Konrad Wachsmann Allee 17, 03046 Cottbus, Germany

[⊥]Ertl Center for Electrochemistry and Catalysis, Gwangju Institute of Science and Technology, 500-712 Gwangju, South Korea

Supporting Information

**ABSTRACT:** Catalytic water splitting to hydrogen and oxygen is considered as one of the convenient routes for the sustainable energy conversion. Bifunctional catalysts for the electrocatalytic oxygen reduction reaction (ORR) and the oxygen evolution reaction (OER) are pivotal for the energy conversion and storage, and alternatively, the photochemical water oxidation in biomimetic fashion is also considered as the most useful way to convert solar energy into chemical energy. Here we present a facile solvothermal route to control the synthesis of amorphous and crystalline cobalt iron oxides by controlling the crystallinity of the materials with changing solvent and reaction time and further utilize these materials as multifunctional catalysts for the unification of photochemical and electrochemical water oxidation as well as for the oxygen reduction reaction. Notably, the amorphous cobalt iron oxide produces superior catalytic activity over the crystalline one under photochemical and electrochemical water oxidation and oxygen reduction conditions.

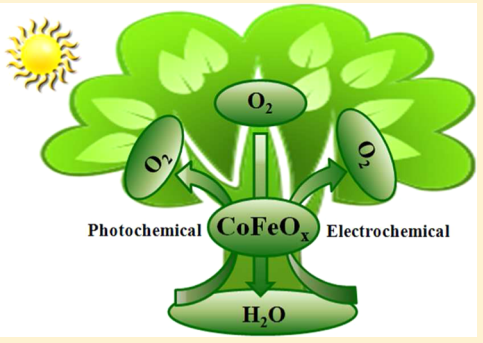


## INTRODUCTION

With increasing demand of global energy production and highly negative impact on the environment from the fossil fuels, it becomes an obvious challenge for modern day science and technology to procure clean and sustainable energy sources.[1] Splitting water to produce hydrogen and oxygen is one convenient way for energy conversion.[2] On the other hand, electrochemical oxygen redox reactions are considered to be the key for energy conversion and storage including fuel cells and metal−air batteries.[3] A single catalyst system used for photochemical and electrochemical water oxidation as well as for oxygen reduction was rare until today. A continuous search of bifunctional catalysts for electrochemical oxygen evolving reaction (OER) and oxygen reduction reaction (ORR) saw the light of success only in recent years.[4,5] At the same time, a single heterogeneous catalyst for the photochemical and electrochemical water oxidation has also been developed.[6]

Development of efficient water oxidation catalyst systems with earth-abundant elements still remains the most challenging task for artificial photosynthesis.[7] Several previously reported catalysts for water oxidation contain precious metals as the active species.[8,9] Biomimicking water oxidation with transition metal oxides has been extensively developed and explored for the past 40 years.[10−14] Since oxido bridged calcium and manganese cubical subcluster was found to be the core group of the oxygen evolving center in photosystem II,[15] manganese oxide based catalysts were extensively studied.[11a,b,16] Similarly, cobalt and nickel oxide based catalysts were also developed for the efficient photochemical and electrochemical water oxidation due to their abundance and eco-friendly features.[12,14] Use of ferrite materials for the water oxidation is in increasing demand because of their high abundance, stability, and magnetic properties.[17,18] Fukuzumi et al. reported an efficient photocatalytic water oxidation with nickel ferrite in the presence of $[Ru(bpy)_3]^{2+}$ (bpy = 2,2′-bipyridine) as the photosensitizer and persulfate as the electron acceptor.[19]

On the contrary, platinum based materials are considered as the most active catalysts for the ORR, but they show low efficiencies for the electrochemical water oxidation.[20] Recently, some of us reported the active catalysts for the oxygen reduction reaction based on Pt alloy.[21,22]Although the Pt based alloys (Pt/Au, Pt/Ir)[23] have shown some enhanced electrocatalytic activities in OER, high cost and scarcity of these metals

Received: September 10, 2014
Published: November 21, 2014

   dx.doi.org/10.1021/ja509348t | J. Am. Chem. Soc. 2014, 136, 17530−17536

make the systems far away from commercialization. Therefore, the approaches were taken to lower the amount of noble metal in the catalyst system by introducing transition metals (Fe, Co, Ni)[24] as well as exploring new catalytic materials with comparable electrochemical activities.[25]

In recent years, the transition metal based mixed metal oxides and spinels have been developed for bifunctional OER and ORR.[26] Stability of the mixed metal oxides in alkaline solution makes them highly promising for this purpose.[26,27] Chen et al. described the room temperature synthesis of Co−Mn−O spinels for the electrochemical oxygen reduction and evolution whereas Rios et al. reported the catalytic activities of mixed valence spinel $Mn_xCo_{3-x}O_4$ for both the OER and the ORR.[4b,27] Recently, Dai et al. discovered $Co_3O_4$ on graphene as the bifunctional catalyst for OER and ORR.[28] Takeguchi et al. described the role of layered perovskite oxide $LaSr_3Fe_3O_{10}$ for both OER-ORR that could be utilized for rechargeable metal−air batteries.[29] Hybrids of graphene and $NiCo_2O_4$ or $NiCo_2S_4$ as the bifunctional electrocatalyst have been established very recently.[30] In addition, nitrogen doped nanoporous carbon materials were also designed for the effective OER−ORR.[31]

In the past few years, special interest has grown on the synthesis and application of amorphous materials for electrocatalysis.[32−37] Electrocatalytic OER with amorphous materials exhibited better performance in terms of overpotential and Tafel slope values.[32−34] Recently, we reported a new route for the synthesis of amorphous manganese oxides for the efficient photochemical and electrochemical water oxidation.[35] Few examples of ORR with amorphous materials have also been reported.[36,37] In the literature, the electrochemical deposition[33] and photochemical metal organic deposition (PMOD)[34] have been used as the possible routes for the synthesis of amorphous films only and not suitable for the large scale synthesis of materials. This led us to investigate a potential route for the formation of amorphous materials which is not only scalable but also highly active toward OER and ORR.

Here we present a highly crystalline (CIO-1: $CoFe_2O_4$) and an amorphous (CIO-2: $CoFe_2O_n$, $n$ = ∼3.66) cobalt iron oxide by applying a simple solvothermal process by controlling the crystallinity of the materials with changing solvent and reaction time (see Scheme 1). The as-prepared CIO-1 and CIO-2 materials were then characterized extensively before subjecting them to photochemical and electrochemical water oxidation and ORR. Under photochemical conditions, the amorphous CIO-2 exhibited catalytic activity superior to that of the crystalline CIO-1. As an electrocatalyst, the amorphous CIO-2 also displayed better performance in OER in comparison to the crystalline CIO-1 in terms of lower potential. In addition to OER, a similar trend was also followed by ORR, where the CIO-2 showed lower onset potential along with exceptional stability in the region of diffusion limited current density. Overall, we have now developed a method to control the synthesis of crystalline and amorphous materials that are active and could solve the prime issues encountered in the field of energy conversion and storage technologies.

**Scheme 1. Synthetic Routes for the Preparation of the Catalysts CIO-1 and CIO-2**

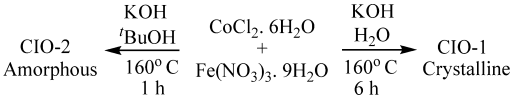


## RESULTS AND DISCUSSION

As amorphous materials have shown promising electrochemical activities,[32−37] our main approach was to develop a large scale and simple synthetic route for the formation of amorphous oxides with high active sites. Therefore, we started with a template free solvothermal procedure and controlled the crystallinity by changing solvent and reaction time. Moreover, we have used simple inorganic salts as the precursors instead of expensive, air and moisture sensitive metal complexes used for PMOD.[34] On the other hand, electrochemical deposition procedures can be applied to form films, and the predetermined control in synthesis is not possible.[33] A well crystalline material (CIO-1) was obtained using water as solvent, whereas in tertiary butanol an amorphous phase (CIO-2) was formed (Scheme 1). In addition to the nature of materials (crystalline or amorphous), significant importance has also been given in literature to understand whether the water oxidation is purely a surface catalyzed reaction or a bulk phenomenon.[15b,38] Recently, the interest has grown to synthesize materials with higher surface area assuming that a larger number active sites are available for water oxidation and oxygen reduction. Interestingly, the Brunauer−Emmett−Teller (BET) surface area of the amorphous CIO-2 (127 $m^2$ $g^{-1}$) is significantly higher (1.5 times) than that of the crystalline CIO-1 (83 $m^2$ $g^{-1}$).

PXRD of CIO-1 belongs to the cubic $CoFe_2O_4$ inverse spinel (Figure 1), and the corresponding (111), (220), (311), (222), (400), (422), (511), (440), (531), (620), (533), (622), and (444) planes were clearly assigned (JCPDS no. 22-1086). PXRD of CIO-2 revealed that the material was amorphous without having any detectable reflections (Figure 1). The chemical compositions of the materials were determined by energy dispersive X-ray (EDX) (Supporting Information Figure S1) and inductively coupled plasma atomic emission spectroscopy (ICP-AES) analyses. The atomic ratios of Co and Fe were determined to be ∼1:2 in both materials. For the amorphous CIO-2, the Co:Fe:O was also determined to be ∼1:2:3.66 from XPS analysis, and the formula could be written as $CoFe_2O_{3.66}$.

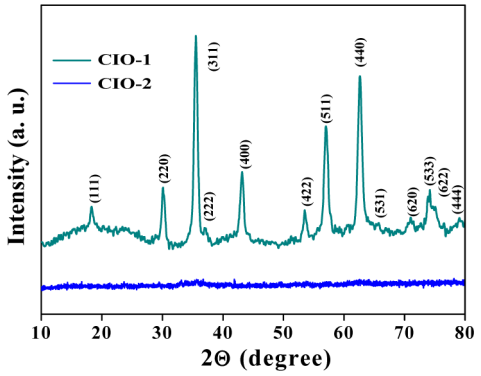


**Figure 1.** Powder XRD patterns of CIO-1 and CIO-2. The reflections from CIO-1 belong to $CoFe_2O_4$ spinel whereas no noticeable reflections were obtained for CIO-2.

The morphology and the size of the particles were determined by TEM analysis (Figure 2). CIO-1 forms cubic type particles with 8−16 nm size, whereas for CIO-2, smaller


dx.doi.org/10.1021/ja509348t | J. Am. Chem. Soc. 2014, 136, 17530−17536

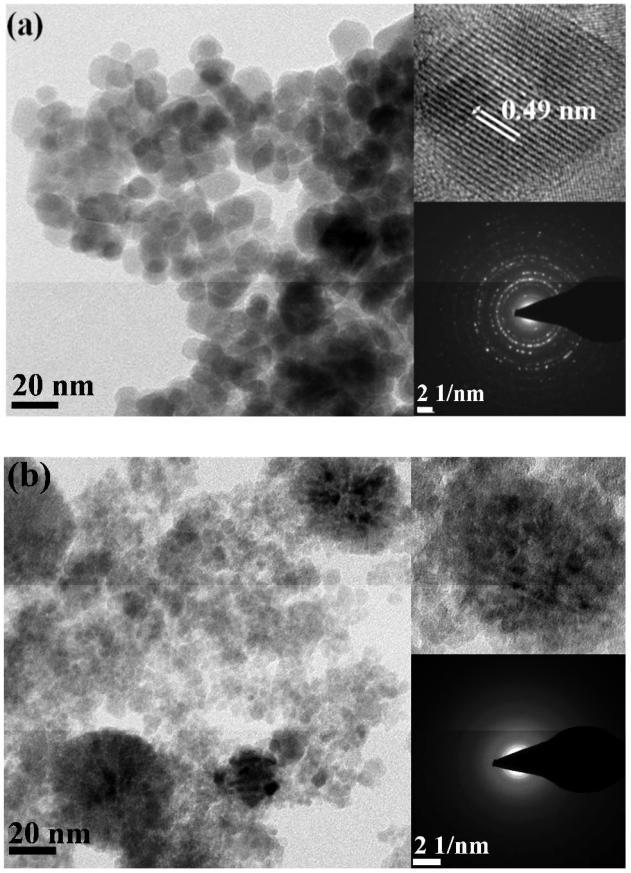


**Figure 2.** TEM images of the catalysts (a) crystalline CIO-1, inset showing the lattices of the crystalline material with lattice spacing of 0.49 nm and selected area diffraction pattern, and (b) amorphous CIO-2, inset figure showing higher resolution image and diffraction pattern.

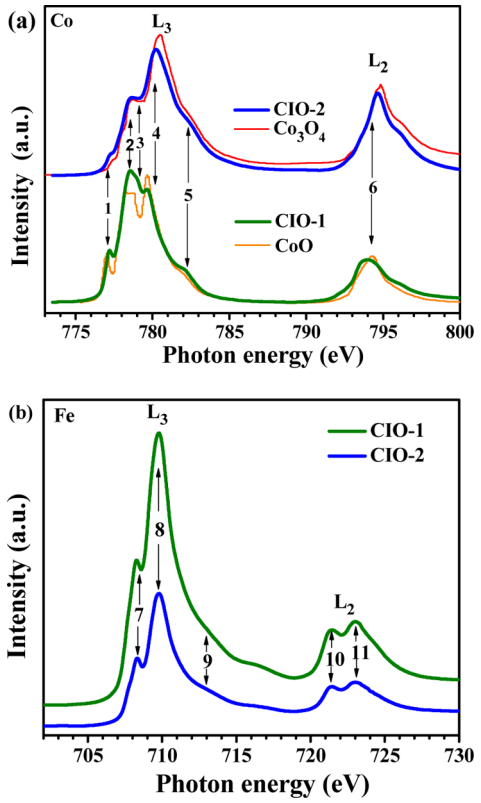


**Figure 3.** X-ray absorption spectra (XAS) of CIO-1 and CIO-2 for (a) Co $L_{2,3}$ edge compared with CoO and $Co_3O_4$ and (b) Fe $L_{2,3}$ edge.

spherical shaped particles (2−8 nm) were observed. The lattice spacing of CIO-1 in the HRTEM image (Figure 2a, right) was determined to be 0.49 nm that corresponds to (111) plane of cubic $CoFe_2O_4$. Selective area diffraction pattern (SAED) also depicted the crystalline nature of CIO-1. Conversely, the HRTEM image of CIO-2 showed clearly an amorphous phase (Figure 2b).

The oxidation states of the elements were first studied by photoemission spectroscopy (PES). The Fe $2p_{3/2}$ spectra of both CIO-1 and CIO-2 were similar, representing the +3 oxidation state of Fe (Supporting Information Figure S2).[39] The Co $2p_{3/2}$ spectra showed the presence of $Co^{2+}$ and $Co^{3+}$, though a substantial difference was observed in the ratio of two oxidation states of CIO-1 and CIO-2 (Supporting Information Figure S2).[40] Further, X-ray absorption spectroscopic (XAS) studies were performed for a deeper understanding of the oxidation and electronic states of each element in the catalysts (Figure 3).

XAS studies of Co $L_{2,3}$ edges of both CIO-1 and CIO-2 catalysts represent two main peaks in energy regions of 778 to 785 eV for $L_3$ edge and 791 to 798 eV for $L_2$ edge. The multiplet splitting causes the fine structures at $L_3$ edges, and the position and intensity of these fine structures are sensitive to the local chemical environment of the oxides. The $L_3$ edge shows five characteristic peaks at 777.1, 778.5, 778.9, 779.8, and 782.2 eV, which is consistent with different valence states in tetrahedral and octahedral symmetry (peaks 1−5 in Figure 3a).

In comparison with reference CoO and $Co_3O_4$ spectra, it is revealed that CIO-1 has higher $Co^{2+}$ contribution than $Co^{3+}$ whereas CIO-2 contains more of $Co^{3+}$.[26a,41] The first three peaks are attributed to $Co^{2+}$ oxidation states and the peaks 4 and 5 to $Co^{3+}$ oxidation states.[42] The Co $L_{2,3}$ spectrum of CIO-1 is consistent with that of inverse spinel $CoFe_2O_4$ where $Co^{2+}$ ions are occupying octahedral sites.[43] Previously, it has been reported that the high spin $Co^{2+}$ configuration contains peaks 2 and 3 with higher intensity compared to peak 4, while the low spin configuration has a reverse behavior.[44,45] In CIO-2, the characteristic higher energy $L_3$ edge peak 4 is more pronounced than that in CIO-1. The ratios of the peaks at the $L_3$ edge are also in good agreement with a mixed occupied spinel ($AB_2O_4$) structure. In addition, the $L_2$ edge peak is shifted to higher energy in CIO-2 as compared to CIO-1. Co $2p_{1/2}$−$2p_{3/2}$ spin−orbit coupling spacing also indicates that the mixed oxidation states are present in CIO-1 and CIO-2.[40b,46]

The XAS spectra of the Fe $L_{2,3}$ edge represent three main peaks at 708.4, 709.7, and a satellite around 713 eV (peaks 7−9 in Figure 3b). The $L_2$ edge shows two peaks of equal intensity (peaks 10−11). The spectra of both CIO-1 and CIO-2 resembles the previously reported Fe $L_{2,3}$ edge spectrum of $CoFe_2O_4$.[43] The peak at 708.4 eV signifies the presence of octahedral sites of $Fe^{2+}$, whereas ∼710 eV represents both octahedral and tetrahedral sites of $Fe^{3+}$.[43] In addition, the spectra are also comparable to that of $\alpha$-$Fe_2O_3$ or $Fe_3O_4$.[47,48]

Additionally, the total amount of reducible sites was determined using temperature-programmed reduction (TPR) in $H_2$. The total amount of reducing sites determined from the area integration revealed that CIO-2 (26%) has more reducible sites than CIO-1 (19%) which is consistent with XAS where more $Co^{3+}$ is present in CIO-2 (Supporting Information Figure


dx.doi.org/10.1021/ja509348t | J. Am. Chem. Soc. 2014, 136, 17530−17536

S3). The resistivities of CIO-1 and CIO-2 were also measured using a four-probe resistivity setup, and the value obtained for crystalline material ($9.1 \pm 0.2 \times 10^6$ Ohm·cm) was significantly lower than that of amorphous material ($1.2 \pm 0.2 \times 10^8$ Ohm·cm).

The well characterized materials were tested for photochemical water oxidation reaction. Water oxidation is a thermodynamically uphill reaction with the transfer of four electrons and four protons. Since the synthesized materials were not photoactive, $[Ru(bpy)_3]^{2+}$ was used as the photosensitizer with $Na_2S_2O_8$ as the electron acceptor. Holes and electrons were generated on the surface of the catalyst after the absorption of the photon by the sensitizer. The electrons were consumed by persulfate, and holes help in the oxidation of water to oxygen (Supporting Information Figure S4). The amount of dissolved $O_2$ was measured by a Clark oxygen electrode system. No oxygen was detected when $[Ru(bpy)_3]^{2+}$ and $Na_2S_2O_8$ were used in the presence of light confirming that involvement of catalyst is essential to produce oxygen.

The total amount of oxygen produced for CIO-1 was ~16 $mmol_{(O2)}$ $mol_{(cat)}^{-1}$ in the first 200 s whereas for CIO-2 it is ~60 $mmol_{(O2)}$ $mol_{(cat)}^{-1}$ (Figure 4). Catalytic activities of CIO-1 and CIO-2 were compared with the commercially available single metal oxides CoO and $Fe_2O_3$ that shows that the mixed metal oxides are more efficient for photochemical water oxidation in phosphate buffer of pH 7.2. To compare with a previously reported $NiFe_2O_4$ catalyst used for the photochemical water oxidation, we synthesized the material and tested it in our setup.[19] The total mass activity of CIO-1 was ~3 times better than $NiFe_2O_4$ whereas CIO-2 showed ~11 times increment.

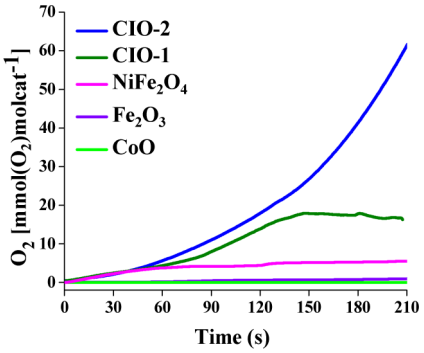


**Figure 4.** Oxygen evolution profiles for the photochemical water oxidation with CIO-1, CIO-2, $NiFe_2O_4$, and commercial CoO, $Fe_2O_3$ using $[Ru(bpy)_3]^{2+}$ as the photosensitizer, and persulfate as the electron acceptor in the presence of 300 W Xe lamp with a cut off filter of 420 nm at 20 °C.

As described earlier, the surface area and the number of active sites of the catalyst play a crucial role in water oxidation. The $O_2$ evolution normalized with BET surface area produces $2.09 \times 10^{-3}$ $mmol_{(O2)}$ $m^{-2}_{(surface)}$ for CIO-2 whereas CIO-1 generates $8.2 \times 10^{-4}$ $mmol_{(O2)}$ $m^{-2}_{(surface)}$ in 200 s. This shows that the amorphous material produces ~2.4 times better activity compared to the crystalline material, even after the surface normalization. It should be mentioned here that CIO-2 also contains a higher amount of low spin $Co^{3+}$ species. Previously, it has been evidenced that the $Co^{3+}$ in the octahedral site facilitates the oxygen evolution reaction, and $Co^{2+}$ is tetrahedral sites were proposed to be inactive for the OER.[26b,30a,49] In addition, recently, a better performance of $Zn^{2+}Co^{3+}{}_2O_4$ than $Co^{2+}Co^{3+}{}_2O_4$, reported by Choi and co-workers also displayed that $Co^{2+}$ in the tetrahedral site remains inactive during oxygen evolution.[50] Thus, better catalytic activity of CIO-2 can be explained by the combination of higher surface area as well as the presence of more of $Co^{3+}$ in octahedral sites.

Long-term photochemical water oxidation in the presence of $Na_2S_2O_8$ as the sacrificial electron acceptor has certain disadvantages due to consumption of peroxodisulfate in the reaction cycle with significant decomposition in the presence of light (Supporting Information Figure S4).[38a,51,52] In addition, the photosensitizer $[Ru(bpy)_3]^{2+}$ is also unstable long-term in the reaction mixture. For a stable catalyst system, the activity could be regained by adding sacrificial agent and photosensitizer.[51,52] For this purpose, we checked the particle morphology after the first run of experiment and no agglomeration was observed for CIO-1 by TEM analysis (Supporting Information Figure S5). Particles became more dispersed after the photochemical experiment in the case of amorphous material (Supporting Information Figure S6). Therefore, the $O_2$ evolution with both catalysts has been further studied for the second run with addition of $[Ru(bpy)_3]^{2+}$ and $Na_2S_2O_8$ in the reaction mixture after the completion of the first run of the photochemical reaction. A significant amount of $O_2$ was detected that proved the stability of the catalyst in the reaction mixture (Supporting Information Figure S7).

The electrochemical activity of CIO-1 and CIO-2 with respect to the water oxidation reaction was measured in 0.1 M potassium hydroxide solution using cyclic voltammetry (CV) at semi-stationary conditions with a scan rate of 6 mV $s^{-1}$ (Figure 5). The electrocatalytic oxygen evolution started at an electrode potential of ~+1.6 V vs RHE, and the anodic current density reached 400 mA $mg^{-1}$ at a potential of +1.74 V for CIO-2 and 370 mA $mg^{-1}$ at +1.84 V for CIO-1. The mass activity of the amorphous CIO-2 material clearly outperformed that of the ordered CIO-1 material over the entire water oxidation potential range (1.5 V to 1.8 V). Electrochemical oxygen evolution also depends largely on the surface area of the catalyst. The CV after normalization by BET surface area reveals that the current density for the crystalline material reaches 19 mA $m_{(surface)}^{-2}$ and for the amorphous material is 14 mA $m_{(surface)}^{-2}$ (Supporting Information Figure S8). However, CIO-2 requires 490 mV to reach a current density of 10 mA $m_{(surface)}^{-2}$ whereas 560 mV is required for the crystalline CIO-1. This confirms the better performance of the amorphous

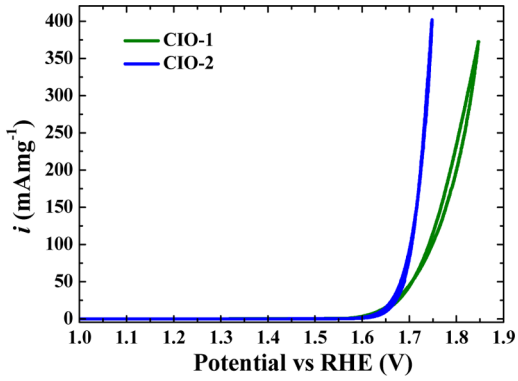


**Figure 5.** Cyclic voltammograms (CV) of CIO-1 and CIO-2 in 0.1 M potassium hydroxide with a scan rate of 6 mV $s^{-1}$.


dx.doi.org/10.1021/ja509348t | J. Am. Chem. Soc. 2014, 136, 17530−17536

material in terms of overpotential in comparison to the crystalline phase.

The Tafel slopes were determined from quasi-stationary experiments. Potential−log[$i$] profiles showed a linear relation in the potential range of +1.50 and +1.65 as well as +1.65 and +1.78 V for both materials. Tafel slope of 48 mV $dec^{-1}$ for CIO-2 and 61 mV $dec^{-1}$ for CIO-1 in lower current density region and substantial increase of 89 mV $dec^{-1}$ was observed for CIO-2 compared to 41 mV $dec^{-1}$ for CIO-1 (Supporting Information Figure S9).

The stability of the catalysts was compared by potentiostatic electrolysis in 0.1 M KOH at +1.75 V (Supporting Information Figure S10). Improved sustained electrochemical stability of the crystalline CIO-1 material was observed compared to the amorphous catalyst CIO-2. The enhanced loss in electrocatalytic activity of the amorphous CIO-2 can be plausibly linked to a more rapid loss in active sites due to structural changes or loss of material from the electrode. In this context, we examined the catalysts after electrolysis (at constant potential of 1.75 V for 30 min in 0.1 M KOH) in a relaxed state by TEM analysis. Formation of an amorphous layer was clearly seen on the surface of the crystalline CIO-1 nanoparticles (Supporting Information Figure S11). This type of observation has been already reported previously by us and by other groups.[12a,25a,45b] Rearrangement of atoms on the surface of the catalyst under high anodic potential and alkaline pH led to the formation of this amorphous layer that indeed acts as the active catalyst for the oxygen evolution. The crystallinity of CIO-1 was retained after electrolysis except for the change on the surface (Supporting Information Figure S11d). For the amorphous CIO-2, highly dispersible ultrasmall particles (∼1−2 nm) were observed by HRTEM (Supporting Information Figure S12). The amorphous nature of the particles was also confirmed by the selected area diffraction (Supporting Information S12d). Ultrasmall particles led to the catalyst loss during long-term electrolysis, resulting in lower stability and a decrease in the current density over time.

As our earlier work reveals that the surface of the catalysts after the electrochemical measurements could result into a different composition and structure, we carried out the X-ray photoelectron spectroscopic (XPS) measurements after the chronoamperometry to understand the surface phenomena.[12a] Comparing Co 2p edges of the fresh sample and after electrochemistry, peak broadening and shifting toward higher energy was observed for both amorphous as well as crystalline materials (Supporting Information Figures S13a and S14a). This indicates the increase in the concentration of $Co^{3+}$ after chronoamperometry, and similar observation was also resulted for Fe 2p peaks (Supporting Information Figures S13b and S14b). More conclusive evidence was obtained from the O 1s edge for CIO-1 and CIO-2, which can be deconvoluted into three main peaks. Two lower energy peaks were attributed for metal−oxygen−metal bonds and surface oxide species[26a] while the highest energy peaks at ∼532 eV indicated the concentrations of the hydroxide species and were significantly increased after electrochemistry for both catalysts (Supporting Information Figures S13c and S14c). Therefore, from XPS analysis, it is clear that a significant amount of surface hydroxide and oxyhydroxide species were formed under the anodic potential and high pH and the obtained results are consistent with other reports with first row transition metal oxide catalysts.[12a]

Electrochemical oxygen reduction ability of pure CIO is poor, and therefore, 20% CIO on carbon (Vulcan X-72) was prepared and characterized (Supporting Information Figures S15−S16). The BET surface area after the loading on Vulcan was determined to be 136 $m^2\ g^{-1}$ for CIO-1 and 140 $m^2\ g^{-1}$ for CIO-2. Catalytic activities for the electrochemical reduction of molecular oxygen (ORR) for the carbon loaded materials were tested by linear sweep voltammetry (LSV) in $N_2$- and $O_2$-saturated electrolytes (Figure 6). The catalytic ORR performances of the mixed metal oxides were compared with commercial carbon-supported Platinum (20 wt % Pt on Vulcan X-72) as a reference. Both CIO-1 and CIO-2 showed catalytic ORR activity. The ORR activity of CIO-2 was significantly higher as reflected by its more positive onset potential (+0.8 V compared to +0.74 V for CIO-1), where a negative (cathodic) faradaic current density emerged, indicating the reduction of oxygen molecules.

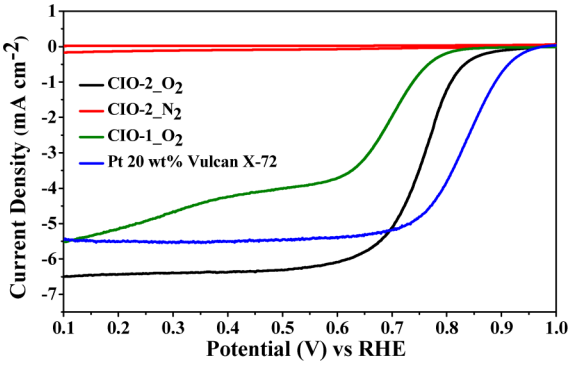


**Figure 6.** Linear sweep voltammetry (LSVs) of CIO-1 and CIO-2 compared with 20 wt % Pt/Vulcan X-72 as reference catalyst in $O_2$-saturated electrolyte in 0.1 M KOH (1600 rpm, 10 mV $s^{-1}$ scan rate) at room temperature.

Unlike CIO-2, the diffusion-limited current density of CIO-1 did not reach the expected value. Our data suggests that on a geometric surface area basis the amorphous CIO-2 material more efficiently catalyzes the transfer of electrons from the electrode to molecular oxygen. The observed ORR activities also surpasses those of previously reported ferrite or cobaltite catalyst materials.[30] Earlier, $Fe_3O_4$ based materials have been explored for the effective oxygen reduction,[53] and improvement of catalytic activity by substitution of iron sites with $Co^{2+}$ and $Mn^{3+}$ have been reported.[54] Use of amorphous mixed metal oxide for the ORR with high efficiency is rare.

To analyze electrochemical kinetic parameters of the amorphous CIO-2 material, we performed an Koutecky−Levich (K−L) analysis to evaluate the number of transferred electrons (Supporting Information Figure S17). On the basis of the K−L plot, the number of transferred electrons was estimated to be close to 4 which is consistent with a selective reduction of molecular $O_2$ to $H_2O$. Comparison of the electrochemical Tafel slope of CIO-2 and the Pt reference catalysts revealed a steeper slope for the non-noble catalysts reflecting a rapid surge in overpotential needed for increasing current densities (Supporting Information Figure S18). The difference in the initial slopes is indicative for difference in the detailed mechanistic pathway of the four electrons on the amorphous materials compared to the Pt surface.

The electrochemical stability of the CIO-1 and CIO-2 during ORR in alkaline conditions was evaluated and compared to a

reference Pt/C catalyst (Supporting Information Figure S19). The activity normalized to the initial activity as a function of time served as a criterion for catalyst stability. Over 100 min, the ORR activity of catalysts CIO-1 and CIO-2 maintained 92% and 94% of their initial values, respectively.

## CONCLUSIONS

In summary, we demonstrated the control over the synthesis of crystalline and amorphous cobalt iron mixed metal oxides starting from simple inorganic salts. Superior performance of the amorphous material was observed in photochemical water oxidation in comparison with the crystalline one. In addition, both the mixed cobalt iron oxides attained far better catalytic activities than $NiFe_2O_4$, CoO, or $Fe_2O_3$. Electrocatalytic water oxidation followed the same trend as photochemical water oxidation by exhibiting lower overpotential for the amorphous material. Increase in the catalytic activity of the amorphous material in terms of onset potential and diffusing limiting current density has also been observed in electrocatalytic $O_2$ reduction reaction. Especially, the amorphous catalyst achieved significantly higher catalytic performance in the kinetics regime. The amorphous catalyst simultaneously owns promising catalytic activity for the ORR and for the OER over the crystalline material. Altogether, our study clearly introduces the scalable synthesis of amorphous and crystalline materials with higher activity that acts as a multifunctional catalyst for the unification of photochemical and electrochemical water oxidation and oxygen reduction.

## ASSOCIATED CONTENT

### Supporting Information

Experimental details, spectroscopic data, electrochemical measurements. This material is available free of charge via the Internet at http://pubs.acs.org.

## AUTHOR INFORMATION


### Corresponding Authors

pstrasser@tu-berlin.de
matthias.driess@tu-berlin.de


### Notes

The authors declare no competing financial interest.

## ACKNOWLEDGMENTS

Authors would like to acknowledge Mr. Patrick Littlewood for the TPR measurements. XAS measurements from BESSY and financial supports from the BMBF (L2H project) and the DFG (Cluster of Excellence UniCat) are gratefully acknowledged. P.S. acknowledges support by the German Federal Ministry of Education and Research under the grant reference number 03SF0433A “MEOKATS”.

## REFERENCES


(1) (a) Chu, S.; Majumdar, A. *Nature* **2012**, *488*, 294−303. (b) Gust, D.; Moore, T. A.; Moore, A. L. *Acc. Chem. Res.* **2009**, *42*, 1890−1898. (c) McAlpina, J. G.; Sticha, T. A.; Caseya, W. H.; Britt, R. D. *Coord. Chem. Rev.* **2012**, *256*, 2445−2452.

(2) (a) Gray, H. B. *Nat. Chem.* **2009**, *1*, 7−7. (b) Eisenberg, R. *Science* **2009**, *324*, 44−45.

(3) Liang, Y.; Li, Y.; Wang, H.; Dai, H. *J. Am. Chem. Soc.* **2013**, *135*, 2013−2036.

(4) (a) Gorlin, Y.; Jaramillo, T. F. *J. Am. Chem. Soc.* **2010**, *132*, 13612−13614. (b) Cheng, F.; Shen, J.; Peng, B.; Pan, Y.; Tao, Z.; Chen, J. *Nat. Chem.* **2011**, *3*, 79−84.

(5) Sa, Y. J.; Kwon, K.; Cheon, J. Y.; Kleitz, F.; Joo, S. H. *J. Mater. Chem. A* **2013**, *1*, 9992−10001.

(6) (a) Grzelczak, M.; Zhang, J.; Pfrommer, J.; Hartmann, J.; Driess, M.; Antonietti, M.; Wang, X. *ACS Catal.* **2013**, *3*, 383−388. (b) Parmar, K. P. S.; Kang, H. J.; Bist, A.; Dua, P.; Jang, J. S.; Lee, J. S. *ChemSusChem* **2012**, *5*, 1926−1934. (c) Klahr, B.; Gimenez, S.; Fabregat, S. F.; Bisquert, J.; Hamann, T. W. *Energy Environ. Sci.* **2012**, *5*, 7626−7636.

(7) (a) Du, P.; Eisenberg, R. *Energy Environ. Sci.* **2012**, *5*, 6012−6021. (b) Rosen, J.; Hutchings, G. S.; Jiao, F. *J. Am. Chem. Soc.* **2013**, *135*, 4516−4521.

(8) (a) Trasatti, S. *Electrochim. Acta* **1984**, *29*, 1503−1512. (b) Zhang, Y.; Judkins, E. C.; McMillin, D. R.; Mehta, D.; Ren, T. *ACS Catal.* **2013**, *3*, 2474−2478. (c) Zhang, Y.; Ren, T. *Chem. Commun.* **2012**, *48*, 11005−11007. (d) Fang, Y. H.; Liu, Z. P. *J. Am. Chem. Soc.* **2010**, *132*, 18214−18222. (e) Indra, A.; Menezes, P. W.; Schwarze, M.; Driess, M. *New J. Chem.* **2014**, *38*, 1942−1945.

(9) (a) Johnson, B.; Girgsdies, F.; Weinberg, G.; Rosenthal, D.; Knop-Gericke, A.; Schlögl, R.; Reier, T.; Strasser, P. *J. Phys. Chem. C* **2013**, *117*, 25443−25450. (b) Busch, M.; Ahlberg, E.; Panas, I. *J. Phys. Chem. C* **2013**, *117*, 288−292. (c) Reier, T.; Oezaslan, M.; Strasser, P. *ACS Catal.* **2012**, *2*, 1765−1772. (d) Blakemore, J. D.; Schley, N. D.; Lenhoff, M. N. K.; Winter, A. M.; D'Souza, F.; Crabtree, R. H.; Brudvig, G. W. *Inorg. Chem.* **2012**, *51*, 7749−7763. (e) Neyerlina, K. C.; Bugosha, G.; Forgiea, R.; Liua, Z.; Strasser, P. *J. Electrochem. Soc.* **2009**, *156*, B363−B369.

(10) (a) Singh, A.; Spiccia, L. *Coord. Chem. Rev.* **2013**, *257*, 2607−2622. (b) Dau, H.; Limberg, C.; Reier, T.; Risch, M.; Roggan, S.; Strasser, P. *ChemCatChem* **2010**, *2*, 724−761.

(11) (a) Bergmann, A.; Zaharieva, I.; Dau, H.; Strasser, P. *Energy Environ. Sci.* **2013**, *6*, 2745−2755. (b) Mette, K.; Bergmann, A.; Tessonnier, J.-P.; Hävecker, M.; Yao, L.; Ressler, T.; Schlögl, R.; Strasser, P.; Behrens, M. *ChemCatChem* **2012**, *4*, 851−862. (c) Najafpour, M. M.; Haghighi, B.; Ghobadi, M. Z.; Sedigh, D. J. *Chem. Commun.* **2013**, *49*, 8824−8826. (d) Fekete, M.; Hocking, R. K.; Chang, S. L. Y.; Italiano, C.; Patti, A. F.; Arena, F.; Spiccia, L. *Energy Environ. Sci.* **2013**, *6*, 2222−2232. (e) Singh, A.; Hocking, R. K.; Chang, S. L.-Y.; George, B. M.; Fehr, M.; Lips, K.; Schnegg, A.; Spiccia, L. *Chem. Mater.* **2013**, *25*, 1098−1108. (f) Zhou, F.; Izgorodin, A.; Hocking, R. K.; Armel, V.; Spiccia, L.; MacFarlane, D. R. *ChemSusChem* **2013**, *6*, 643−651.

(12) (a) Pfrommer, J.; Lublow, M.; Azarpira, A.; Göbel, C.; Lücke, M.; Steigert, A.; Pogrzeba, M.; Menezes, P. W.; Fischer, A.; Schedel-Niedrig, T.; Driess, M. *Angew. Chem., Int. Ed.* **2014**, *53*, 5183−5187. (b) Blakemore, J. D.; Gray, H. B.; Winkler, J. R.; Muller, A. M. *ACS Catal.* **2013**, *3*, 2497−2500. (c) Ko, J. W.; Ryu, W. H.; Kim, I. D.; Park, C. B. *Chem. Commun.* **2013**, *49*, 9725−9727. (d) Lu, X.; Zhao, C. *J. Mater. Chem. A* **2013**, *1*, 12053−12059. (e) Maitra, U.; Naidu, B. S.; Govindaraj, A.; Rao, C. N. R. *Proc. Natl. Acad. Sci. U. S. A.* **2013**, *110*, 11704−11707.

(13) (a) Young, K. M. H.; Klahr, B. M.; Zandi, O.; Hamann, T. W. *Catal. Sci. Technol.* **2013**, *3*, 1660−1671. (b) Hou, Y.; Zuo, F.; Dagg, A.; Feng, P. *Angew. Chem., Int. Ed.* **2013**, *52*, 1248−1252. (c) Klahr, B.; Gimenez, S.; Fabregat, S. F.; Hamann, T.; Bisquert, J. *J. Am. Chem. Soc.* **2012**, *134*, 4294−4302.

(14) (a) Cristino, V.; Berardi, S.; Caramori, S.; Argazzi, R.; Carli, S.; Meda, L.; Tacca, A.; Bignozzi, C. A. *Phys. Chem. Chem. Phys.* **2013**, *15*, 13083−13092. (b) Singh, A.; Chang, S. L. Y.; Hocking, R. K.; Bach, U.; Spiccia, L. *Catal. Sci. Technol.* **2013**, *3*, 1725−1732. (c) Sun, K.; Pang, X.; Shen, S.; Qian, X.; Cheung, J. S.; Wang, D. *Nano Lett.* **2013**, *13*, 2064−2072. (d) Singh, A.; Chang, S. L. Y.; Hocking, R. K.; Bach, U.; Spiccia, L. *Energy Environ. Sci.* **2013**, *6*, 579−586. (e) Fukuzumi, S.; Hong, D.; Yamada, Y. *J. Phys. Chem. Lett.* **2013**, *4*, 3458−3467. (f) Sun, K.; Park, N.; Sun, Z.; Zhou, J.; Wang, J.; Pang, X.; Shen, S.; Noh, S. Y.; Jing, Y.; Jin, S.; Yu, P. K. L.; Wang, D. *Energy Environ. Sci.* **2012**, *5*, 7872−7877.

(15) (a) Hocking, R. K.; Brimblecombe, R.; Chang, L. Y.; Singh, A.; Cheah, M. H.; Glover, C.; Casey, W. H.; Spiccia, L. *Nat. Chem.* **2011**, *3*, 461−466. (b) Robinson, D. M.; Go, Y. B.; Mui, M.; Gardner, G.;

Zhang, Z.; Mastrogiovanni, D.; Garfunkel, E.; Li, J.; Greenblatt, M.; Dismukes, G. C. *J. Am. Chem. Soc.* **2013**, *135*, 3494−3501.
(16) (a) Baktash, E.; Zaharieva, I.; Schroeder, M.; Goebel, C.; Dau, H.; Thomas, A. *Dalton Trans.* **2013**, *42*, 16920−16929. (b) Kim, Y. Y.; Williams, D.; Meldrum, F. C.; Walsh, D. *Small* **2013**, *9*, 61−66. (c) Zaharieva, I.; Najafpour, M. M.; Wiechen, M.; Haumann, M.; Kurz, P.; Dau, H. *Energy Environ. Sci.* **2011**, *4*, 2400−2408. (d) Najafpour, M. M.; Ehrenberg, T.; Wiechen, M.; Kurz, P. *Angew. Chem., Int. Ed.* **2010**, *49*, 2233−2237.
(17) Trotochaud, L.; Ranney, J. K.; Williams, K. N.; Boettcher, S. W. *J. Am. Chem. Soc.* **2012**, *134*, 17253−17261.
(18) (a) Louie, M. W.; Bell, A. T. *J. Am. Chem. Soc.* **2013**, *135*, 12329−12337. (b) Chen, S.; Qiao, S. Z. *ACS Nano* **2013**, *7*, 10190−10196.
(19) Hong, D.; Yamada, Y.; Nagatomi, T.; Takai, Y.; Fukuzumi, S. *J. Am. Chem. Soc.* **2012**, *134*, 19572−19575.
(20) (a) Winter, M.; Brodd, R. J. *Chem. Rev.* **2004**, *104*, 4245−4270. (b) Wu, G.; Zelenay, P. *Acc. Chem. Res.* **2013**, *46*, 1878−1889.
(21) Cui, C.; Gan, L.; Heggen, M.; Rudi, S.; Strasser, P. *Nat. Mater.* **2013**, *12*, 765−771.
(22) (a) Strasser, P.; Koh, S.; Anniyev, T.; Greeley, J.; More, K.; Yu, C.; Liu, Z.; Kaya, S.; Nordlund, D.; Ogasawara, H.; Toney, M. F.; Nilsson, A. *Nat. Chem.* **2010**, *2*, 454−460. (b) Cui, C.; Gan, L.; Li, H.; Yu, S.; Heggen, M.; Strasser, P. *Nano Lett.* **2012**, *12*, 5885−5889.
(23) (a) Lu, Y.-C.; Xu, Z.; Gasteiger, H. A.; Chen, S.; Hamad-Schifferli, K.; Shao-Horn, Y. *J. Am. Chem. Soc.* **2010**, *132*, 12170−12171. (b) Yang, J.; Chen, X.; Yang, X.; Ying, J. Y. *Energy Environ. Sci.* **2012**, *5*, 8976−8981. (c) Kong, F. D.; Zhang, S.; Yin, G. P.; Zhang, N.; Wang, Z. B.; Du, C. Y. *J. Power Sources* **2012**, *210*, 321−326. (d) Chen, Z.; Higgins, D.; Yu, A.; Zhang, L.; Zhang, J. *Energy Environ. Sci.* **2011**, *4*, 3167−3192. (e) Zhang, G.; Shao, Z. G.; Lu, W.; Li, G.; Liu, F.; Yi, B. *Electrochem. Commun.* **2012**, *22*, 145−148. (f) Zhang, H.; Yang, W. *Chem. Commun.* **2007**, 4215−4217.
(24) (a) Stamenkovic, V. R. *Science* **2007**, *315*, 493−497. (b) Yang, R. Z.; Leisch, J.; Strasser, P.; Toney, M. *Chem. Mater.* **2010**, *22*, 4712−4720. (c) Yang, R. Z.; Strasser, P.; Toney, M. *J. Phys. Chem. C* **2011**, *115*, 9074−9080.
(25) (a) Liang, H. W.; Wei, W.; Wu, Z. S.; Feng, X.; Müllen, K. *J. Am. Chem. Soc.* **2013**, *135*, 16002−16005. (b) Zhang, Y.; Ge, J.; Wang, L.; Wang, D.; Ding, F.; Tao, X.; Chen, W. *Sci. Rep.* **2013**, *3*, 2771.
(26) (a) Menezes, P. W.; Indra, A.; Sahraie, N. S.; Bergmann, A.; Strasser, P.; Driess, M. *ChemSusChem* **2014**, DOI: 10.1002/cssc.201402699. (b) Liang, Y.; Wang, H.; Zhou, J.; Li, Y.; Wang, J.; Regier, T.; Dai, H. *J. Am. Chem. Soc.* **2012**, *134*, 3517−3523. (c) Sugawara, M.; Ohno, M.; Matsuki, K. *J. Mater. Chem.* **1997**, *7*, 833−836. (d) Xu, J.; Gao, P.; Zhao, T. S. *Energy Environ. Sci.* **2012**, *5*, 5333−5339.
(27) Rios, E.; Gautier, J. L.; Poillerat, G. *Electrochim. Acta* **1998**, *44*, 1491−1497.
(28) Liang, Y.; Li, Y.; Wang, H.; Zhou, J.; Wang, J.; Regier, T.; Dai, H. *Nat. Mater.* **2011**, *10*, 780−786.
(29) Takeguchi, T.; Yamanaka, T.; Takahashi, H.; Watanabe, H.; Kuroki, T.; Nakanishi, H.; Orikasa, Y.; Uchimoto, Y.; Takano, H.; Ohguri, N.; Matsuda, M.; Murota, T.; Uosaki, K.; Ueda, W. *J. Am. Chem. Soc.* **2013**, *135*, 11125−11130.
(30) (a) Lee, D. U.; Kim, B. J.; Chen, Z. *J. Mater. Chem. A* **2013**, *1*, 4754−4762. (b) Liu, Q.; Jin, J.; Zhang, J. *ACS Appl. Mater. Interfaces* **2013**, *5*, 5002−5008. (c) Bian, W.; Yang, Z.; Strasser, P.; Yang, R. *J. Power Sources* **2014**, *250*, 196−203.
(31) Lin, Z.; Waller, G. H.; Liu, Y.; Liu, M.; Wong, C. *Carbon* **2013**, *53*, 130−136.
(32) Kanan, M. W.; Nocera, D. G. *Science* **2008**, *321*, 1072−1075.
(33) Tsuji, E.; Imanishi, A.; Fukui, K.-I.; Nakato, Y. *Electrochim. Acta* **2011**, *56*, 2009−20016.
(34) (a) Smith, R. D. L.; Prevot, M. S.; Fagan, R. D.; Zhang, Z.; Sedach, P. A.; Siu, M.; Kit, J.; Trudel, S.; Berlinguette, C. P. *Science* **2013**, *340*, 60−63. (b) Smith, R. D. L.; Prevot, M. S.; Fagan, R. D.; Trudel, S.; Berlinguette, C. P. *J. Am. Chem. Soc.* **2013**, *135*, 11580−11586. (c) Smith, R. D. L.; Sporinova, B.; Fagan, R. D.; Trudel, S.; Berlingguette, C. P. *Chem. Mater.* **2014**, *26*, 1654−1659. (d) Zhang, C.; Trudel, S.; Berlinguette, C. P. *Eur. J. Inorg. Chem.* **2014**, 660−664.
(35) Indra, A.; Menezes, P. W.; Zaharieva, I.; Baktash, E.; Pfrommer, J.; Schwarze, M.; Dau, H.; Driess, M. *Angew. Chem., Int. Ed.* **2013**, *52*, 13206−13210.
(36) Zhou, W.; Ge, L.; Chen, Z.-G.; Liang, F.; Xu, H.−Y.; Motuzas, J.; Julbe, A.; Zhu, Z. *Chem. Mater.* **2011**, *23*, 4193−4198.
(37) Lee, J.-S.; Park, G. S.; Lee, H. I.; Kim, S. T.; Cao, R.; Cho, J. *Nano Lett.* **2011**, *11*, 5362−5366.
(38) (a) Menezes, P. W.; Indra, A.; Littlewood, P.; Schwarze, M.; Göbel, C.; Schomäcker, R.; Driess, M. *ChemSusChem* **2014**, *7*, 2202−2211. (b) Jin, K.; Park, J.; Lee, J.; Yang, K. D.; Pradhan, G. K.; Sim, U.; Jeong, D.; Jang, H. L.; Park, S.; Kim, D.; Sung, N.; Kim, S. H.; Han, S.; Nam, K. T. *J. Am. Chem. Soc.* **2014**, *136*, 7435−7443.
(39) (a) Grosvenor, A. P.; Kobe, B. A.; McIntyre, N. S. *Surf. Sci.* **2004**, *565*, 151−162. (b) Poulin, S.; Franca, R.; Moreau-Belanger, L.; Sacher, E. *J. Phys. Chem. C* **2010**, *114*, 10711−10718.
(40) (a) Chuang, T. J.; Bridle, C. R.; Rice, D. W. *Surf. Sci.* **1976**, *59*, 413−429. (b) Oku, M.; Hirokawa, K. *J. Electron Spectrosc. Relat. Phenom.* **1976**, *8*, 475−481.
(41) Lamirand, A. D.; Soares, M. M.; Ramos, A. Y.; Tolentino, H. C. N.; Santis, M. D.; Cezar, J. C.; Siervo, A.; Jamet, M. *Phys. Rev. B* **2013**, *88*, 140401(1)−140401(5).
(42) (a) Csiszar1, S. I.; Haverkort, M. W.; Hu, Z.; Tanaka, A.; Hsieh, H. H.; Lin, H.-J.; Chen, C. T.; Hibma, T.; Tjeng, L. H. *Phys. Rev. Lett.* **2005**, *95*, 187205. (b) Richter, M.; Schmeißer, D. *Appl. Phys. Lett.* **2013**, *102*, 253904. (c) Casey, W. H. *J. Colloid Interface Sci.* **1991**, *146*, 586−589. (d) Kim, J.-Y.; Park, J.-H.; Park, B.-G.; Noh, H.-J.; Oh, S.-J.; Yang, J. S.; Kim, D.-H.; Bu, S. D.; Noh, T.-W.; Lin, H.-J.; Hsieh, H.-H.; Chen, C. T. *Phys. Rev. Lett.* **2003**, *90*, 017401−3.
(43) Kim, C. H.; Myung, Y.; Cho, Y. J.; Kim, H. S.; Park, S.-H.; Park, J. *J. Phys. Chem. C* **2009**, *113*, 7085−7090.
(44) Regan, T. J.; Ohldag, H.; Stamm, C.; Nolting, F.; Luning, J.; Stohr, J.; White, R. L. *Phys. Rev. B* **2001**, *64*, 214422.
(45) (a) Wang, J.; Zhou, J.; Hu, Y.; Regier, T. *Energy Environ. Sci.* **2013**, *6*, 926−934. (b) Lee, S. W.; Carlton, C.; Risch, M.; Surendranath, Y.; Chen, S.; Furutsuki, S.; Yamada, A.; Nocera, D. G.; Shao-Horn, Y. *J. Am. Chem. Soc.* **2012**, *134*, 16959−16962. (c) Lutterman, D. A.; Surendranath, Y.; Nocera, D. G. *J. Am. Chem. Soc.* **2009**, *131*, 3838−3839.
(46) Lopez, N.; Graham, D. J.; McGuire, R.; Alliger, G. E.; Shao-Horn, Y.; Cummins, C. C.; Nocera, D. G. *Science* **2012**, *335*, 450−453.
(47) (a) Crocombette, J. P.; Pollak, M.; Joliet, F.; Thromat, N.; Gautier, S. M. *Phys. Rev. B* **2013**, *88*, 3143−3150. (b) Cheung, S. H.; Celik-Aktas, A.; Dey, P.; Pande, K.; Weinert, M.; Kabius, B.; Keavney, D. J.; Lazarov, V. K.; Chambers, S. A.; Gajdardziska-Josifovska, M. *Phys. Rev. B* **2012**, *85*, 045405.
(48) (a) Chen, C. L.; Dong, C. L.; Rao, S. M.; Chern, G.; Chen, M. C.; Wu, M. K.; Chang, C. L. *J. Phys.: Condens. Matter* **2008**, *20*, 255236. (b) Moyer, J. A.; Vaz, C. A. F.; Negusse, E.; Arena, D. A.; Henrich, V. E. *Phys. Rev. B* **2011**, *83*, 035121.
(49) (a) Rios, E.; Chartier, P.; Gautier, J.-L. *Solid State Sci.* **1999**, *1*, 267−277. (b) Hamdani, M.; Singh, R. N.; Chartier, P. *Int. J. Electrochem. Sci.* **2010**, *5*, 556−577.
(50) Kim, T. W.; Woo, M. A.; Regis, M.; Choi, K. S. *J. Phys. Chem. Lett.* **2014**, *5*, 2370−2374.
(51) Zhao, Y.; Liu, Y.; Du, X.; Hana, R.; Ding, Y. *J. Mater. Chem. A* **2014**, *2*, 19308−19314.
(52) (a) Jiao, F.; Frei, H. *Energy Environ. Sci.* **2012**, *3*, 1018−1027. (b) Jiao, F.; Frei, H. *Chem. Commun.* **2012**, *46*, 2920−2922.
(53) (a) Su, Y.; Jiang, H.; Zhu, Y.; Yang, X.; Shen, J.; Zou, W.; Chen, J.; Li, C. *J. Mater. Chem. A* **2014**, *2*, 7281−7287. (b) Wu, Z.-S.; Yang, S.; Sun, Y.; Parvez, K.; Feng, X.; Müllen, K. *J. Am. Chem. Soc.* **2012**, *134*, 9082−9085.
(54) Zhan, Y.; Xu, C.; Lu, M.; Liu, Z.; Lee, J. Y. *J. Mater. Chem. A* **2014**, *2*, 16217−16223.